

# Accelerating the Photocatalytic Degradation of Green Dye Pollutants by Using a New Coating Technique for Carbon Nanotubes with Nanolayered Structures and Nanocomposites

Osama Saber,<sup>\*[a, b]</sup> Abdullah Aljaafari,<sup>[a]</sup> Mostafa Osama,<sup>[c]</sup> and Hasan Alabdulgader<sup>[c]</sup>

The present study has two aims, first to accelerate the degradation of pollutants by coating carbon nanotubes (CNTs) with nanoplatelets or nanocomposites of aluminum zinc oxides and second to fabricate an advanced photocatalyst. Accordingly, Zn-Al layered double hydroxides (LDHs) were grown in the presence of functionalized CNTs during urea hydrolysis. The presence of CNTs led to the formation of LDH nanoplatelets, and TEM images showed that the CNTs were coated with nanoplatelets. The nanoplatelets were thermally treated to

form nanocomposite-coated CNTs. Raman spectra demonstrated the successful coating of CNTs with LDHs and nanocomposite. The coated CNTs were very effective in the photocatalytic degradation of industrial pollutants. A kinetics study demonstrated that the rate of photocatalytic degradation of green dye in the presence of CNTs coated with aluminum zinc oxide nanocomposite was five times faster than with the aluminum zinc oxide nanocomposite.

## 1. Introduction

Over 100 000 types of dyes are used annually in the dyeing industry, and more than  $7 \times 10^5$  tons of dyes are manufactured worldwide.<sup>[1,2]</sup> It is known that even low concentrations of dyes can cause health problems in humans and animals. Consequently, in recent decades the elimination of synthetic dyes has become a global problem because of these colorful effluents.<sup>[3,4]</sup> This topic has attracted our attention because it is aimed at accelerating the decomposition of pollutants and also at the discovery of new techniques for coating CNTs with dual metal oxide nanocomposites.


Zinc oxide is one of the most suitable photocatalysts for the photocatalytic degradation of pollutants.<sup>[5]</sup> However, single metal oxides cannot meet all the demands of new technology to accelerate photocatalytic reactions and avoid the disadvantages of photocatalysts.<sup>[6]</sup> In many cases, a combination of two or more metal oxides leads to compounds with superior properties compared with the discrete oxides.<sup>[7,8]</sup> To increase the optical properties and photoactivity of zinc oxide, many researchers have shifted its light absorption onset from the UV region to the visible region by narrowing the bandgap energy.<sup>[7]</sup> This was achieved by introducing metal and nonmetal dopants into the zinc oxide structure. The optical properties of ZnO could be changed by the introduction of extrinsic dopants, such as aluminum, at zinc lattice sites.<sup>[5-8]</sup> Other researchers have tried to achieve this aim by reducing the rate of recombination reactions of photogenerated electron-hole pairs in zinc oxide. They have focused on the use of carbon-based nanofillers, for example, fullerene, carbon nanotubes (CNTs), and graphite, as electron sinks. Of these, CNTs have attracted attention because of their amazing properties, which have prompted a wide range of studies and useful applications.<sup>[9-11]</sup>


The presence of CNTs and ZnO nanoparticles could increase the photocatalytic degradation of acetaldehyde.<sup>[12]</sup> Similarly, zinc oxide supported on CNTs causes cyanide degradation in aqueous media under UV irradiation.<sup>[13]</sup> Suriani et al.<sup>[14]</sup> confirmed the effect of CNTs with zinc oxide through an improvement in field electron emissions. Also, the attachment of CNTs to ZnO caused an increase in electronic and optical properties.<sup>[15]</sup> Yang et al.<sup>[16]</sup> used magnetron sputtering to produce network sensors based on CNTs coated with ZnO nanoparticles. Moyo et al.<sup>[17]</sup> modified a glassy carbon electrode with

[a] Prof. O. Saber, Dr. A. Aljaafari  
Physics Department, Faculty of Science  
King Faisal University  
Al-Hassa 31982, P.O. Box 400 (Saudi Arabia)  
E-mail: osmohamed@kfu.edu.sa

[b] Prof. O. Saber  
Petroleum Refining  
Egyptian Petroleum Research Institute  
Nasr City, P.O. Box 11727, Cairo (Egypt)

[c] M. Osama, Dr. H. Alabdulgader  
Chemical Engineering Department  
College of Engineering  
King Faisal University  
Al-Hassa 31982, P.O. Box 400 (Saudi Arabia)

 The ORCID identification number(s) for the author(s) of this article can be found under:  
<https://doi.org/10.1002/open.201800173>.

 © 2018 The Authors. Published by Wiley-VCH Verlag GmbH & Co. KGaA. This is an open access article under the terms of the Creative Commons Attribution-NonCommercial-NoDerivs License, which permits use and distribution in any medium, provided the original work is properly cited, the use is non-commercial and no modifications or adaptations are made.

CNTs/ZnO composites to act as a gas sensor. More recently, ZnO nanoparticles were supported on the surface of CNTs to improve the field emission characteristics of the CNTs.<sup>[18,19]</sup> CNTs and zinc oxide nanocomposites were synthesized by using a plasma-enhanced chemical vapor deposition method.<sup>[20]</sup> Freire et al.<sup>[21]</sup> reported that the electrocatalytic oxidation of phenolic compounds increased after the morphology of ZnO nanoparticles was changed by bonding with CNTs.

Recently, the efforts of these researchers has directed interest in the development of ZnO-CNTs structures by inserting multiple metals into a combination of CNTs and layered double hydroxides (LDHs). LDHs are a family of two-dimensional layered ordered structures that have confined embedded anions between their layers.<sup>[22,23]</sup> These layers are cationic because of the presence of divalent and trivalent metals in the same layer. These materials appear to be very adaptable, because they give rise to an unlimited range of nanocomposites or doped materials owing to the presence of different metals in ordered and layered structures.

Li et al.<sup>[24]</sup> and Zhao et al.<sup>[25]</sup> used LDHs as catalysts to produce CNTs. Marco et al.<sup>[26]</sup> have supported graphene oxide and CNTs over LDHs for CO<sub>2</sub> adsorption applications. Li et al.<sup>[27]</sup> and Zhang et al.<sup>[28]</sup> used LDH/CNTs as catalysts for oxidation and reduction reactions. Zhang et al.<sup>[29]</sup> synthesized a hybrid supercapacitor comprised of Ni-Al LDHs attached to CNTs. In the field of environmental remediation, studies that depend on a combination of CNTs and LDHs are rare because of unattractive results published by Wang et al.<sup>[30]</sup> and Lan et al.,<sup>[31]</sup> who supported Zn-Al LDHs particles over CNTs but did not get good results for the photocatalytic degradation of pollutants. Lan et al.<sup>[31]</sup> supported small Zn-Al-In LDH particles over CNTs, but their materials did not cause complete photocatalytic degradation of pollutants after irradiation for 4 h. Wang et al.<sup>[30]</sup> supported small particles of hybrid Zn-Al LDHs over CNTs, but these materials did not give complete photocatalytic degradation of pollutants after irradiation for 7 h. These unattractive results may be a result of the use of small amounts of LDHs with CNTs and their combination did not promote the coating of CNTs.

Herein, we present a process for coating Zn-Al LDH nanoplatelets onto CNTs, followed by conversion of the nanoplatelets into an aluminum zinc oxides nanocomposite coating on the CNTs. The coated CNTs were used to fabricate an advanced photocatalyst to accelerate the photocatalytic degradation of pollutants. CNTs coated with aluminum zinc oxide nanocomposite were synthesized and compared with LDHs and aluminum zinc oxide nanocomposite. The effect of CNTs on the optical properties of the LDHs and the nanocomposite was also investigated. Furthermore, the photocatalytic activity of the prepared materials was measured for the degradation of green dye under UV light irradiation. Kinetic studies were used to evaluate the effect of the coated CNTs on the rate of photocatalytic decomposition of the dyes.

## 2. Results and Discussion

### 2.1. Growth of Nanoplatelets to Coat CNTs

The presence of CNTs during the growth of LDHs leads to the formation of particular morphologies and sizes of Zn-Al LDHs.

In the absence of CNTs, LDHs grow by producing large layers and plates, as shown in Figure 1. Large hexagonal plates with dimensions of 500 to 800 nm are observed. From the side, the thickness of the plates is about 390 nm and their lengths are about 2  $\mu\text{m}$ , as shown in Figure 1, inset. In the presence of CNTs, nanoscale LDHs were produced, as shown in Figure 2. Figure 2a,b shows CNTs coated with layers of LDHs. Figure 2c,d shows that the CNTs were coated with LDH nano-

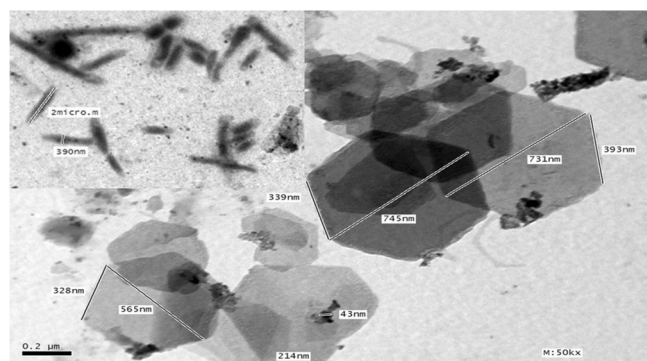


Figure 1. TEM images of conventional Zn-Al LDHs.

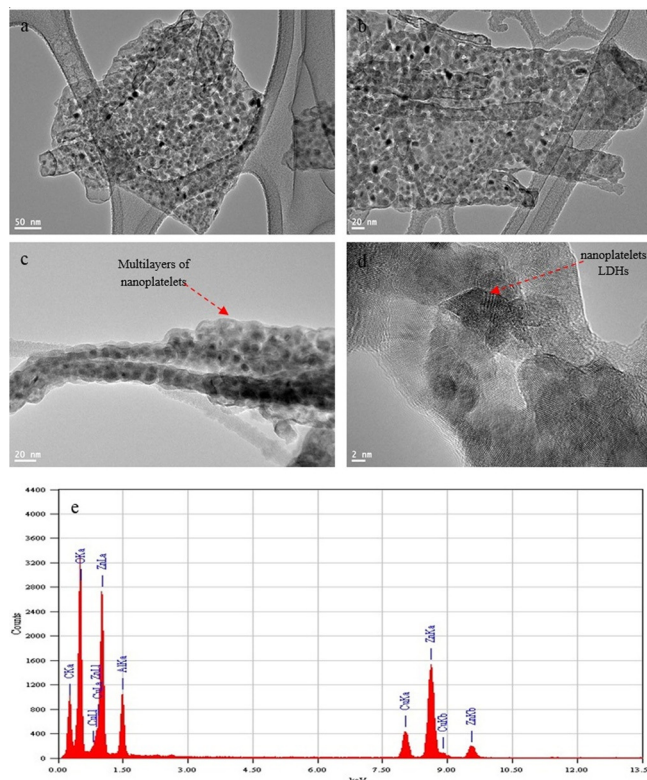


Figure 2. a-d) TEM images and e) EDX spectrum of CNTs-LDHs.

platelets. On magnification, clear hexagonal nanoplatelets with a thickness of around 20 nm were observed (Figure 2d). Also, CNTs coated with multiple layers of nanoplatelets were observed to look like nanofibers (Figure 2c). The TEM results indicated that the growth of LDH nanoplatelets in the presence of CNTs may be considered a new coating technique for CNTs. Energy-dispersive X-ray (EDX) spectroscopy analysis revealed that zinc, aluminum, carbon, and oxygen were clearly present in the LDHs-coated CNTs (Figure 2e).

X-ray diffraction (XRD) was used to characterize the crystal size and layered structure of the prepared Zn-Al LDHs. Figure 3 shows the XRD pattern for the as-prepared CNTs-LDHs, in which two series of layered structures can be seen. The first

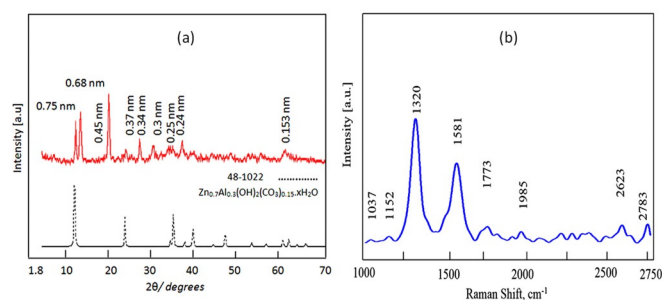


Figure 3. a) XRD and b) Raman spectrum of CNTs-LDHs.

has three peaks at 0.75, 0.37, and 0.25 nm. These three peaks are related to the reflections of the (003), (006), and (009) planes, in agreement with the standard data for Zn-Al carbonate LDHs (JCPDS no. 48-1022). Additionally, a characteristic peak for the (110) plane was observed at 0.153 nm. These results indicated that being coated onto CNTs did not affect the layered structures of LDHs because  $d_{(003)} = 2d_{(006)} = 3d_{(009)}$ . Furthermore, the metal-metal distance within the layers, as calculated from the relationship  $a = 2d_{(110)}$ , did not change. The second series shows another three peaks at 0.68, 0.34, and 0.23 nm, which agree with the LDHs structure after drying (without interlayered water).<sup>[32]</sup> This shows that the presence of CNTs during the growth of LDHs restricted the extension of the LDH layers. Therefore, some LDH crystals did not have enough space for interlayered water.

The XRD results confirmed that CNTs-LDHs have two spacings at 0.75 and 0.68 nm, and thus these LDHs have layered structures with two different sizes. According to the Scherer equation,<sup>[33]</sup> these sizes are 54 and 31 nm. These results confirmed that the platelets of LDHs are on the nanoscale, which agrees with the TEM images. The characteristic peak of CNTs was observed at  $2\theta \approx 26^\circ$ , attributed to the C (002) plane,<sup>[25]</sup> and is overlapped by the LDH peaks. In addition, there is a clear peak at  $2\theta = 20^\circ$ . It is characteristic of polyvinyl alcohol (PVA) and represents reflections from the (101) plane and an interlayer spacing of 0.45 nm.<sup>[34]</sup>

To study the effect of LDHs on the CNTs, the Raman spectrum of the LDHs-coated CNTs is shown in Figure 3b. The spectrum mainly showed two bands at 1320 (D band) and 1581  $\text{cm}^{-1}$  (G band). The G band originates from the Raman-

active  $E_{2g}$  mode due to in-plane atomic displacements. The origin of the D band is explained as disorder-induced features due to the lattice distortion. The D band is frequently referred to as the defect band. Its intensity relative to the G band is often used to determine the quality of nanotubes. The  $I_D/I_G$  ratio of pure CNTs is 0.8 to 0.9,<sup>[35,36]</sup> whereas the ratio for CNTs-LDHs was 1.6, which indicates an enhancement in the D peak relative to pure CNTs. This enhancement is believed to be due to disorders and defects associated with the process of coating LDHs onto CNTs.

The Raman spectrum of CNTs-LDHs also exhibited a band at 2623  $\text{cm}^{-1}$ , which was assigned to the 2D band that corresponds to a double-resonance Raman process and is characteristic of multiwalled CNTs.<sup>[30]</sup> Other weak bands in the spectrum are due to the LDH structure.

To study the effect of CNTs on the structure of LDHs, the IR spectra of Zn-Al LDHs with and without CNTs were recorded and are shown in Figure 4. The stretching of hydroxyl groups

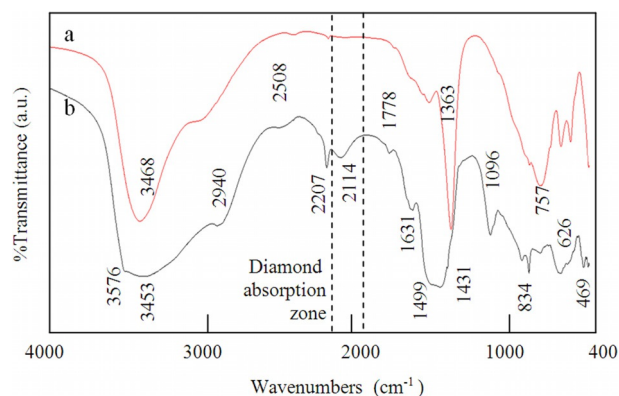


Figure 4. FTIR spectra of a) conventional LDHs and b) CNTs-LDHs.

in pure Zn-Al LDH was observed at 3468  $\text{cm}^{-1}$ , as shown in Figure 4a. Figure 4b shows that CNTs-LDHs have two bands at 3453 and 3576  $\text{cm}^{-1}$ , which indicates the presence of two different hydroxyl groups, in agreement with the XRD and TEM results. The growth of LDH nanoplatelets on the CNTs resulted in a band at 3453  $\text{cm}^{-1}$ , and the interaction between the LDH nanoplatelets and the CNTs affected the stretching vibrations of the O-H groups and resulted in a shift in the band to 3576  $\text{cm}^{-1}$ . A similar effect was also observed for interlayered carbonate anions, that is, the strong, sharp band at 1362  $\text{cm}^{-1}$ , assigned to carbonate anions in pure LDH, was split into two bands at 1431 and 1499  $\text{cm}^{-1}$  in the spectrum of CNTs-LDHs. One band is due to interlayered carbonate anions inside the LDH nanoplatelets around the CNTs and the other is assigned to carbonate anions that are interacting with CNTs. Furthermore, a clear band was observed at 2114  $\text{cm}^{-1}$ , which confirmed the presence of CNTs.

The changes in the characteristic spectral bands of the hydroxyl groups and carbonate anions of LDHs with and without CNTs reflect the effective role of CNTs in controlling the morphology of LDHs, and indicate the existence of chemical interactions between the CNTs and LDHs.<sup>[29]</sup> This may be explained



by the presence of hydrogen bonds between the hydroxyl groups of the LDHs and the functional groups of CNTs (-COOH). This speculation could be confirmed by the broadness of the O-H band and a shoulder at around  $2940\text{ cm}^{-1}$  owing to hydrogen-bonding interactions.<sup>[29,37]</sup> The band at around  $1631\text{ cm}^{-1}$  was assigned to the bending vibration of interlayer water molecules, which agrees with the presence of hydrogen bonds.<sup>[37]</sup> The peak at  $2207\text{ cm}^{-1}$  suggested the presence of cyanate as the secondary interlayered anion. The peaks in the low-wavenumber region ( $834$ ,  $757$ ,  $626$ , and  $469\text{ cm}^{-1}$ ) were mainly due to various lattice vibrations associated with metal hydroxide sheets.<sup>[29]</sup> These results showed that two different kinds of nanoplatelets were successfully grown: some nanoplatelets interact with CNTs and others grow as multilayers around the CNTs.

Thermogravimetric (TG) and differential scanning calorimetry (DSC) analyses were used to study the thermal decomposition behavior of CNTs-LDHs. The TG curve showed a two-step decomposition on heating under an inert nitrogen atmosphere. The first step occurred in two stages, as shown in Figure 5a.

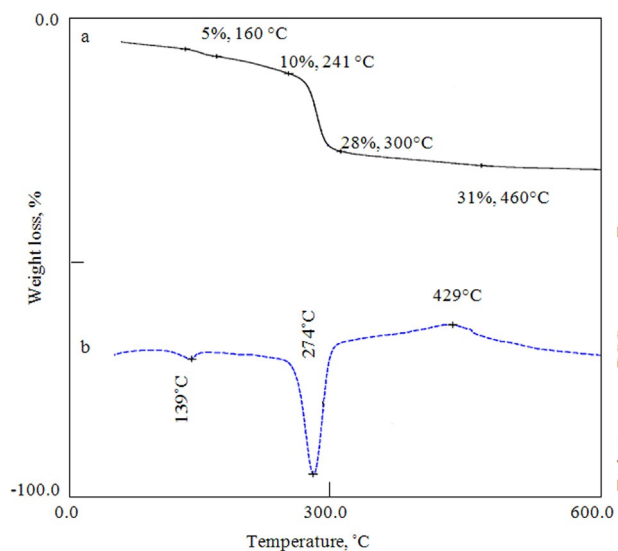


Figure 5. a) TG and b) DSC analyses of CNTs-LDHs.

The first and second stages occurred at  $160$  and  $241\text{ °C}$ , respectively, and accounted for a  $10\%$  weight loss due to the release of both physisorbed and interlayered water in addition to the decomposition of polyvinyl alcohol.<sup>[37]</sup> The second step took place in two stages above  $241\text{ °C}$  and resulted in a  $21\%$  weight loss. The first stage was observed at  $300\text{ °C}$  and was due to decomposition of the interlayer anions. The second stage was due to the dehydroxylation of LDH layers and was detected at  $460\text{ °C}$ . The DSC curve exhibited two endothermic peaks, as shown in Figure 5b, which agrees with the TG results. In addition, one exothermic peak was observed at  $429\text{ °C}$ , which indicated complete conversion of the LDHs to a nanocomposite and the resulting crystallization energy.

## 2.2. Coating CNTs with Nanocomposite

Based on the results of the thermal analyses of CNTs-LDHs, the nanolayered structures of LDHs are converted to a nanocomposite after heating above  $460\text{ °C}$ . Therefore, CNTs-LDHs were thermally treated at  $500\text{ °C}$ .

XRD analysis of the treated CNTs-LDHs indicated that the layered LDH structures had disappeared (Figure 6a). All the diffraction lines were identified as the zinc oxide wurtzite structure (JCPDS no. 36-1451) by fitting and matching them with typical diffraction patterns of zincite phases. In addition, the

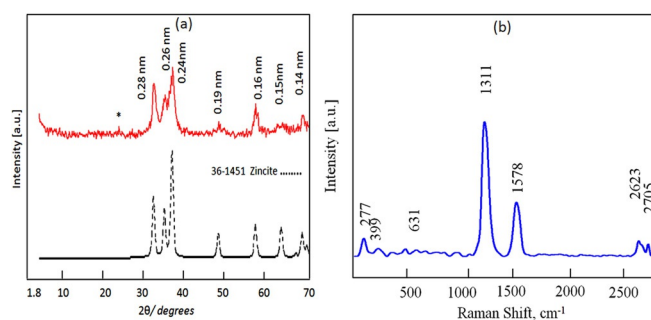


Figure 6. a) XRD and b) Raman spectrum of nanocomposite-coated CNTs.

broadness of the diffraction lines suggested that the particles were nanosized. According to the Scherer equation,<sup>[36]</sup> the size of these nanoparticles was  $11\text{ nm}$ . Also, the XRD pattern showed no peaks for aluminum oxide (Figure 6a), which indicated that aluminum was homogeneously dispersed inside the ZnO wurtzite structure as a dopant. In addition, a weak peak related to the (002) plane of CNTs was observed at  $2\theta = 26\text{ °}$ . The weakness of this peak suggested that the CNTs were completely covered by aluminum zinc oxide nanocomposite.

The Raman spectrum of the treated CNTs-LDHs was recorded in the range of  $250$  to  $2800\text{ cm}^{-1}$  to examine the structures of the CNTs and the aluminum zinc oxide nanocomposite. As shown in Figure 6b, three prominent bands are clearly visible at  $1311$ ,  $1578$ , and  $2623\text{ cm}^{-1}$ , and correspond to the D, G, and 2D bands of CNTs, respectively. In addition, weak bands for aluminum zinc oxide were observed below  $1000\text{ cm}^{-1}$ . The intensity ratio of the D and G bands ( $I_D/I_G$ ) was  $2.5$ , indicative of more disordered carbon in the treated CNTs-LDHs. The G peak position of the treated CNTs-LDHs ( $1578\text{ cm}^{-1}$ ) exhibited a shift to lower frequency ( $\approx 3\text{ cm}^{-1}$ ) compared with untreated CNTs-LDHs ( $1581\text{ cm}^{-1}$ ). In general, hybrid carbon nanomaterials exhibit this type of low-frequency shift (softening) when functionalized with an electron-donor molecule.<sup>[35,38]</sup> The lower frequency shift observed for the treated CNTs-LDHs confirmed the charge transfer between the nanocomposite and the CNTs, in which aluminum zinc oxide acts as an electron donor and CNTs act as an electron acceptor. This lower-frequency shift and the higher ratio of the D and G band intensities revealed the functionalization and coating of CNTs with aluminum zinc oxide nanocomposite and confirmed their vital role in accelerating photocatalytic reactions (discussed below). This explana-

tion agrees with the findings of previous researchers, who reported that the G band shifted to a lower wavenumber and the  $I_D/I_G$  ratio increased when CNTs were coupled with metal oxides because of the electron-donor characteristics of metal toward the CNTs.<sup>[39–41]</sup>

In addition, the peaks below  $1000\text{ cm}^{-1}$  in the spectrum of the nanocomposite-coated CNTs, which are related to the Raman-active modes of the metal oxides, demonstrated the successful integration of the nanocomposite onto the CNTs.<sup>[42,43]</sup>

Figure 7 shows TEM images of the treated CNTs-LDHs, which revealed the nanofiber shape of the aluminum zinc oxide nanocomposite. Figure 7a,c (inset) shows that the nanoparticles formed from the decomposition of the nanoplatelets aggregated and connected together around the CNTs. This indicates that thermal decomposition of the CNTs-LDHs transformed the LDH nanoplatelets into nanoparticles of aluminum-doped zinc oxide, that is, nanoparticles started to grow and aggregate at a high temperature in the presence of CNTs, and the CNTs acted as seeds to collect nanoparticles around them (see Figure 7). These results agree with the XRD and Raman spectroscopy data, and confirm that thermal treatment converted CNTs-LDHs into nanocomposite-coated CNTs. EDX analysis revealed that zinc, aluminum, carbon, and oxygen could be clearly identified in the nanocomposite-coated CNTs (Figure 7e).

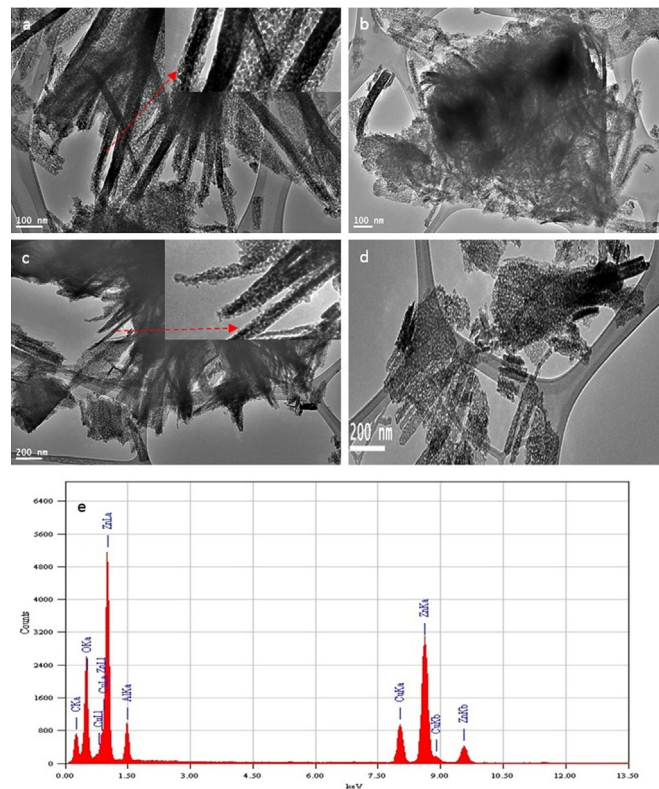


**Figure 7.** a–d) TEM images and e) EDX spectrum of nanocomposite-coated CNTs.

### 2.3. Optical Properties and Photoactivity

It is known that pure zinc oxide has a wide bandgap energy (3.37 eV). Figure 8 shows the bandgaps and absorbance spectra for CNTs coated with LDHs or aluminum zinc oxide nanocomposite in the range of  $\lambda = 200$  to 400 nm. The sharp in-

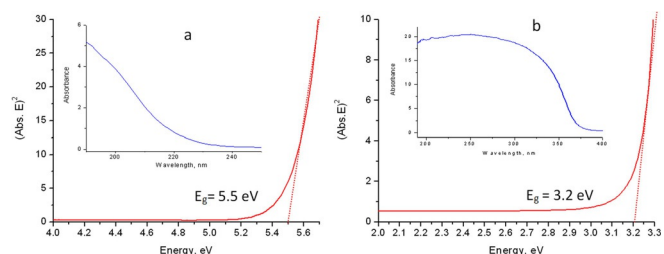


**Figure 8.** Optical properties of a) CNTs-LDHs and b) nanocomposite-coated CNTs.

crease at the blue end of the spectrum is due to the excitation of electrons from the valence band ( $V_B$ ) to the conduction band ( $C_B$ ). Therefore, the absorption data, which matches the electronic excitation from the  $V_B$  to the  $C_B$ , could be used to calculate the energy bandgap ( $E_g$ ). The relationship between the absorption coefficient (Abs) and the incident photon energy ( $E = h\nu$ ) is defined in Equation (1):<sup>[3,5]</sup>

$$(\text{Abs } E)^m = A(E - E_g) \quad (1)$$

in which  $m$  is an index that defines the optical absorption process and is 1/2 or 2 for allowed indirect or allowed direct transitions, respectively, and  $A$  is a constant. For aluminum zinc oxide, a direct electronic transition occurs from oxygen  $2p$  to the metal  $ns$  or  $np$  levels ( $n=4$  for Zn and  $n=3$  for Al), which indicates that  $m=2$ .

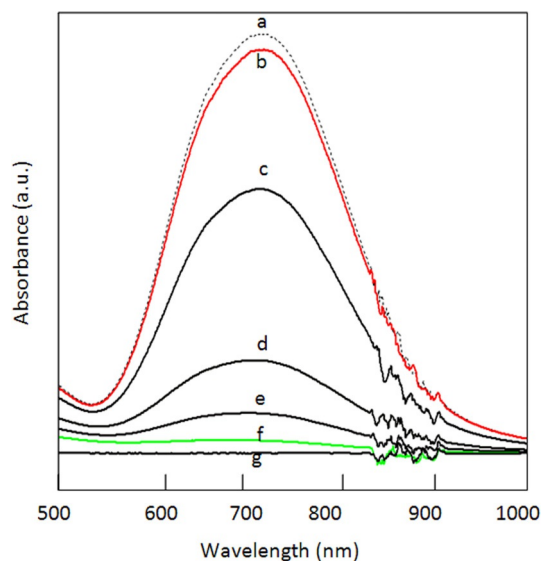
Thus, by plotting  $(\text{Abs } E)^2$  and  $(E)$ , the bandgap could be calculated by extending the straight line to the axis ( $E$ ) to determine the bandgap energy of the samples at  $(\text{Abs } E)^2 = 0$ , as shown in Figure 8.

Figure 8a shows that the  $E_g$  value for CNTs-LDHs is 5.5 eV. After converting CNTs-LDHs to nanocomposite-coated CNTs, the absorbance spectrum moved to the visible region and the bandgap value became 3.2 eV, as shown in Figure 8b. That is, the bandgap of bulk ZnO narrowed from 3.37 to 3.20 eV in the aluminum zinc oxide nanocomposite-coated CNTs. Compared with our previous results for aluminum zinc oxide nanoparticles without CNTs,<sup>[5]</sup> a small narrowing of the bandgap from 3.23 to 3.20 eV was observed for nanocomposite-coated CNTs. This may be because of the coating of aluminum-doped zinc oxide onto CNTs.

To evaluate the effect of CNTs on the photoactivity of Zn-Al LDHs and aluminum zinc oxide nanocomposite, the photoactivity of both CNTs-LDHs and nanocomposite-coated CNTs were studied and compared with LDHs and aluminum-doped zinc oxide nanoparticles in the photocatalytic degradation of naphthol green B (NGB).

The intensity of the absorption of green dye at  $\lambda_{\max} = 714$  nm indicates the concentration. A blank experiment, performed without any solid catalyst materials, revealed the stability of NGB under UV light. When an aqueous mixture of green dye and the catalyst material was kept in the dark for 1 h, a slight variation was noticed. To avoid the effects of other factors in the process, this was considered to be 0 h irradiation.

An aqueous mixture of green dye and one of the prepared nanostructures was irradiated with UV light, and the photocatalytic decomposition of green dyes was noted as a function of irradiation time. These results are presented in Figures 9 and 10. The percentage of green dye in the presence of CNTs-LDHs



**Figure 9.** Absorption spectra of NGB ( $4 \times 10^{-4}$  M) in the presence of CNTs-LDHs after irradiation with UV light for a) 0, c) 0.3, d) 1.4, e) 2.1, f) 2.8, and g) 4.5 h; b) no light.

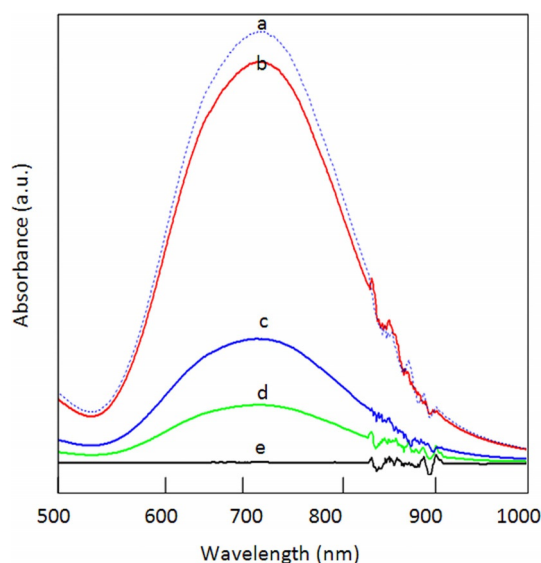


**Figure 10.** Absorption spectra of NGB ( $4 \times 10^{-4}$  M) in the presence of nano-composite-coated CNTs after irradiation with UV light for a) 0, c) 0.3, d) 0.7, and e) 1.25 h; b) no light.

under UV light decreased as the irradiation time was increased, and complete disappearance of NGB dye was observed after 4.5 h (Figure 9). This indicated that complete decomposition of the green pollutant had occurred, leading to decolorization of the mixture.

By transforming the LDHs-coated CNTs into nanocomposite-coated CNTs, complete decolorization and degradation of the green dye were achieved after an irradiation time of 1.25 h; the plot in Figure 10 shows the complete disappearance of green dye. This shows that the aluminum zinc oxide nanocomposite-coated CNTs were very effective because they completely destroyed the green dye in a shorter time than nanoparticles of aluminum-doped zinc oxide,<sup>[5]</sup> which degraded the green dye after over 6 h.<sup>[5]</sup>

#### 2.4. Mechanism of the CNTs Coating Process

Based on the XRD, IR spectroscopy, thermal analyses, and TEM results, we suggest a mechanism to understand the growth of nanoplatelets on the CNTs.

Initially, the LDH nanolayers started to grow in the presence of functionalized CNTs. The formation of hydrogen bonds between hydroxyl groups (-OH) on the LDHs and the functional groups (-COOH) of the CNTs, as confirmed by the IR spectra and thermal analyses, restricted the growth of the LDH platelets. PVA, which has a lot of hydroxyl groups, acted as a binder between the CNTs and LDHs. The restricted growth process of LDHs on CNTs limited the extension of the LDH platelets and prevented the LDHs nanolayers from agglomerating, which directed the formation of LDH nanoplatelets as seen in the TEM images (Figure 2). In addition, hydrogen bonds between the CNTs and the rigid nanoplatelets caused elongation of the CNTs, as seen in the TEM images. We concluded that CNTs could act as seeds or heterogeneous nucleation sites for the growth of layered structures of Zn-Al LDHs to build multilayers of nanoplatelets that coated the CNTs.

After thermal decomposition of Zn-Al LDHs at 500 °C, the LDH nanoplatelets were transformed into nanoparticles of aluminum-doped zinc oxide and the PVA was converted into carbon dioxide and water. At high temperature, the aluminum-doped zinc oxide nanoparticles started to aggregate and build layers of nanocomposite onto the CNTs, as shown in the TEM images.

#### 2.5. Mechanism of Fast Degradation of Pollutants

The high performance of the aluminum zinc oxide nanocomposite-coated CNTs as a photocatalyst could be explained by studying the mechanism of photocatalytic reactions, which depend mainly on two processes (I and II), as shown in Figure 11. Process I is an excitation, in which incident photons with energies higher than the energy of the bandgap cause excitation of electrons from the  $V_B$  to the  $C_B$  [Reaction (R1)]. Accordingly, positive holes ( $h^+$ ) start to collect in the  $V_B$ . These positive holes oxidize the pollutants or react with water molecules to produce highly oxidizing  $\cdot OH$  free radicals. At the same time, excited electrons in the  $C_B$  reduce oxygen mole-



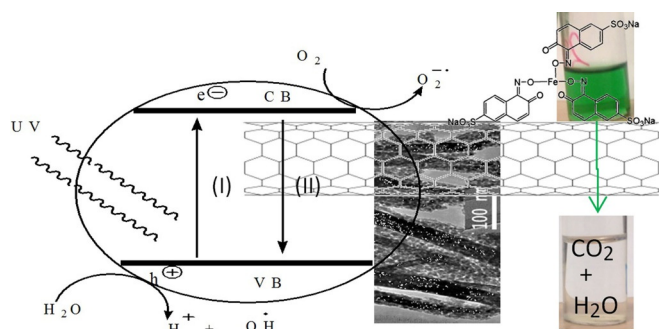


**Figure 11.** The mechanism for the accelerated photocatalytic degradation of pollutants by nanocomposite-coated CNTs.

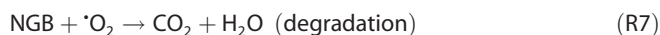
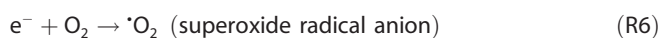
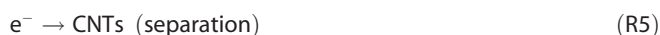
cules adsorbed on the photocatalyst surface to produce strong oxidizing agents. Process II is a recombination, in which excited electrons return to the  $V_B$  and recombine with the positive holes, which results in a weakening of process I and the photoactivity of the catalyst.

Aluminum zinc oxide nanoparticle photocatalysts have narrow and limited areas because they are zero-dimensional materials. The process of electron accumulation in the  $C_B$  of these nanoparticles is shown in Reaction (R2). This accumulation results in an increase in the rate of recombination process (II), as indicated in Reaction (R3). Accordingly, Reaction (R3) weakens photocatalytic degradation reactions.

In the presence of aluminum-doped zinc oxide nanoparticles, the following reactions occur:



In the presence of nanocomposite-coated CNTs, Reactions (R4), (R5), (R6), and (R7) take place:



In the aluminum zinc oxide nanocomposite-coated CNTs photocatalyst, electrons could be easily excited and transferred from the  $V_B$  to the  $C_B$  by UV light irradiation because the aluminum and CNTs reduced the bandgap of zinc oxide from 3.37 to 3.20 eV and accordingly accelerated process I. Another effect of the CNTs, which have extremely high electron conductivity because of their small diameter and huge length/diameter ratio, is that excited electrons in the  $C_B$  of the aluminum zinc oxide nanocomposite could be quickly transported along the graphitic structure of the CNTs to react and oxidize adsorbed pollutants. This means that the presence of CNTs in contact with aluminum zinc oxide cancels the accumulation

process [Reaction (2)] through a separation process [Reaction (5)]. Therefore, the rate of the recombination reaction (process II) was very low. Also, the photoexcited electrons were delocalized and the mobility of the generated electrons increased because of the presence of CNTs. Accordingly, photoexcited electrons could react with oxygen molecules to produce superoxidizing agents that strongly attacked the dye in different locations at the same time, as indicated in Reactions (6) and (7). This mechanism explains the high ability of the aluminum zinc oxide nanocomposite-coated CNTs to destroy the pollutants in a short time under UV light.

To confirm the effect of coating CNTs with LDH nanoplatelets or aluminum zinc oxide nanocomposite, the kinetics of the photocatalytic decolorization and degradation of green dye were studied for CNTs-LDH and nanocomposite-coated CNTs. The kinetics of the decolorization and degradation of the dye can be represented by Equation (2):

$$\ln[A_0]/[A_t] = kt \quad (2)$$

in which  $[A_0]$  is the absorbance at  $t=0$ ,  $[A_t]$  is the absorbance at time  $t$ , and  $k$  is the rate constant. The kinetics of the decolorization and degradation of dye with LDH-coated CNTs and nanocomposite-coated CNTs under UV light are presented in plots of  $\ln[A_0]/[A_t]$  versus irradiation time, as shown in Figure 12.

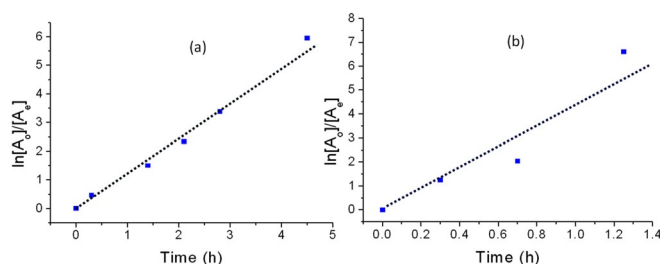


**Figure 12.** Typical kinetics obtained for the photocatalytic degradation of NGB in the presence of a) CNTs-LDHs and b) nanocomposite-coated CNTs.

From Figure 12a, it could be inferred that the decolorization and degradation of dye under UV light with CNTs-LDH as the photocatalyst exhibited pseudo-first-order behavior with a rate constant of  $1.2 \text{ h}^{-1}$ . Compared with recently reported conventional Zn-Al LDHs (without CNTs),<sup>[3]</sup> the rate constant for the photocatalytic degradation of green dye in the presence of CNTs-LDHs was higher. Thus, the coating of CNTs with LDHs accelerates the photocatalytic degradation. With aluminum zinc oxide nanocomposite-coated CNTs the rate constant was  $4.1 \text{ h}^{-1}$ , which is five times higher than Al-doped zinc oxide nanoparticles, as previously published by our laboratory,<sup>[5]</sup> for the decolorization and photodegradation of green dye.

The kinetic study confirmed that CNTs coated with LDHs or nanocomposite increased the reaction rate of the photocatalytic degradation of the dyes.

Finally, the coating of CNTs with Al-doped zinc oxide led to a dual effect. The first effect is acceleration of the excitation

process through narrowing of the bandgap energy of the photocatalyst. The second effect is a weakening of the recombination process by a reduction in the accumulation of electrons in the  $C_B$  through quick transport of the excited electrons from the  $C_B$  to the CNTs to react with adsorbed dyes. Therefore, the degradation and decolorization of green dyes occurred in a short time (1.25 h).

### 3. Conclusions

The present study achieved the dual aims of coating CNTs with LDH nanoplatelets or aluminum zinc oxide nanocomposite and producing effective photocatalysts to accelerate the photocatalytic degradation of industrial pollutants.

CNTs were coated with nanoplatelets of Zn-Al LDHs and, after thermal treatment, these nanoplatelets were transformed into aluminum zinc oxide nanocomposite nanolayers that coated the CNTs. After coating the CNTs, two positive effects were observed. The first effect was acceleration of the excitation of electrons from the  $V_B$  of the aluminum zinc oxide nanocomposite to the  $C_B$ . It was achieved by narrowing the bandgap energy of the photocatalyst from 3.37 to 3.20 eV. The second effect was a weakening of the recombination of the photogenerated electron-hole pairs of the nanocomposite. It was accomplished by avoiding the accumulation of electrons in the  $C_B$  by quick transport of excited electrons from the  $C_B$  to the CNTs to react with the adsorbed dyes. Therefore, nanocomposite-coated CNTs were very active in the photocatalytic decomposition of pollutants. This activity was observed by the decolorization and decomposition of green dye in a short time; 1.25 h with aluminum zinc oxide nanocomposite-coated CNTs. Compared with aluminum zinc oxide nanoparticles, the photocatalytic degradation of green dye was five times faster with the nanocomposite-coated CNTs photocatalyst because of the dual effect of CNTs coated with nanocomposite. The kinetic study confirmed that CNTs coated with LDHs or nanocomposite accelerated the reaction rate of the photocatalytic degradation of the dyes.

In conclusion, the dual effect of aluminum zinc oxide nanocomposite-coated CNTs is very important to produce an effective photocatalyst for the degradation of industrial pollutants.

## Experimental Section

### Coating of the CNTs

Functionalized CNTs and other chemicals were provided by Sigma-Aldrich. CNTs-Zn-Al LDHs were precipitated by urea hydrolysis. Zinc nitrate (0.05 mol) and aluminum nitrate (0.02 mol) were used as metal precursors and urea (0.05 mol) acted as the precipitant and pH control. The temperature of the reaction was held at 90 °C for 12 h. Polyvinyl alcohol was used to facilitate the coating of CNTs during growth of the LDH nanolayers because PVA is a water-soluble polymer that is widely used as a binder.<sup>[44]</sup> Distilled water was used to wash the final product, which was then dried at RT under vacuum for 24 h. For simplicity, the product was called CNTs-LDHs. For comparison, Zn-Al LDHs were also prepared without CNTs.

CNTs-LDHs were converted into nanocomposite-coated CNTs by thermal treatment at 500 °C.

### Physical Measurements

Imaging of the prepared samples at the nanoscale was achieved by using TEM with JEM 2100F instrument. EDX spectroscopy was performed by using an Electron Probe Micro analyzer JED 2300 instrument. XRD analysis was carried out by using a Bruker-AXS instrument (Karlsruhe, Germany;  $Cu_{K\alpha}$  radiation,  $\lambda = 0.154$  nm). FTIR spectroscopy was performed as KBr discs in the range of 425–4000  $cm^{-1}$  by using a Perkin-Elmer Spectrum 400 instrument. DSC and TG analyses were carried out under nitrogen gas by using TA series Q 500 and Q 600 instruments, respectively. Raman spectroscopy measurements were performed by using a Lab RAM HR Evolution instrument (Horiba-Jobin-Yvon) equipped with a 633 ULF laser and a grating groove density of 300 grooves  $mm^{-1}$ . UV/Vis absorption spectroscopy was performed by using the diffuse reflectance technique to measure the optical parameters of the nanomaterials by using a UV/VIS/NIR Shimadzu 3600 spectrophotometer. The spectrophotometer was equipped with an integrating sphere attachment (ISR-603) to measure solid materials, and the thickness of the sample was 3 mm. Barium sulfate was used as the reflectance standard.

### Photocatalytic Reactions

The photocatalytic activity of the different nanostructures was examined for the decomposition of industrial green dyes. The oxidants that formed on the surface of the nanostructures during irradiation with UV light could react and oxidize the green pollutants to be colorless. At low concentrations of the dye, the concentration is directly proportional to the intensity of the measured spectrum of the dye. Herein, an aqueous solution of NGB ( $4 \times 10^{-4}$  M) in the presence of the prepared nanostructures (0.1 g) was exposed to UV light by using a 400 W mercury lamp. Photocatalytic reactions were performed at RT in a cylindrical glass vessel equipped with an immersion UV lamp, a magnetic stirrer, and a cooling system to avoid thermal reactions. The characteristic peak of NGB is at  $\lambda = 714$  nm. The extent of degradation was calculated from the integrated area of the peak at  $\lambda = 714$  nm. Before illumination, the mixture was stirred for 30 min to reach the adsorption-desorption equilibrium of NGB on the catalyst. The following photocatalytic degradation of the pollutants was checked by extracting small portions of the solution at different time intervals. The decolorization and decomposition of the dye were monitored by following the decline in its concentration in the aqueous solution. A UV/Vis spectrophotometer was used to measure the dye concentration before and after irradiation.

### Acknowledgements

The authors thank the Deanship of Scientific Research in King Faisal University (Saudi Arabia) for funding and providing the facilities required for this research as a part of the Research Grants Program (no. 17122002).

### Conflict of Interest

The authors declare no conflict of interest.



**Keywords:** dyes/pigments · layered compounds · nanostructures · nanotubes · photochemistry

- [1] D. Jyothi, P. Deshpande, B. R. Venugopal, S. Chandrasekaran, G. Madras, *J. Chem. Sci.* **2012**, *124*, 385–393.
- [2] Y. Li, J. Kuang, Y. Lu, W. Cano, *Acta Metall. Sin. (Engl. Lett.)* **2017**, *30*, 1017–1032.
- [3] O. Saber, H. Alomair, M. Abu-Abdeen, A. Aljaafari, *Acta Metall. Sin. (Engl. Lett.)* **2018**, *31*, 533–546.
- [4] C. Liu, H. Xu, L. Wang, X. Qin, *Acta Metall. Sin. (Engl. Lett.)* **2017**, *30*, 36–44.
- [5] O. Saber, T. A. El-Brolosy, A. A. Aljaafari, *Water Air Soil Poll.* **2012**, *223*, 4615–4626.
- [6] K. Karunakaran, P. Gomathisankar, G. Manikandan, *Mater. Chem. Phys.* **2010**, *123*, 585–594.
- [7] D. Ya-Juan, L. Yi, L. Jin-Ku, Y. Xiao-Hong, *J. Alloy. Compd.* **2015**, *648*, 438–444.
- [8] J. Wang, J. Liu, Q. Tong, Y. Lu, X. Yang, *Ind. Eng. Chem. Res.* **2014**, *53*, 2229–2237.
- [9] G. Mittal, V. Dhand, K. Y. Rhee, S. J. Park, W. R. Lee, *J. Ind. Eng. Chem.* **2015**, *21*, 11–25.
- [10] S. Y. Lee, D. H. Kim, S. C. Choi, D. J. Lee, J. Y. Choi, H. D. Kim, *Microporous Mesoporous Mater.* **2014**, *194*, 46–51.
- [11] S. Safa, *Opt. Int. J. Light Electron. Opt.* **2015**, *126*, 2194–2198.
- [12] T. A. Saleh, M. Gondal, Q. Drmosh, *Nanotechnology* **2010**, *21*, 495705–495713.
- [13] T. A. Saleh, M. Gondal, Q. Drmosh, Z. Yamani, A. Al-Yamani, *Chem. Eng. J.* **2011**, *166*, 407–412.
- [14] A. Suriani, R. Safitri, A. Mohamed, S. Alfarisa, I. Isa, A. Kamari, N. Hashim, M. Ahmad, M. Malek, M. Rusop, *Mater. Lett.* **2015**, *149*, 66–69.
- [15] L. Kong, X. Yin, M. Han, L. Zhang, L. Cheng, *Ceram. Int.* **2015**, *41*, 4906–4915.
- [16] M. Yang, H. C. Kim, S. H. Hong, *Mater. Lett.* **2012**, *89*, 312–315.
- [17] M. Moyo, L. R. Florence, J. O. Okonkwo, *Sens. Actuators B* **2015**, *209*, 898–905.
- [18] M. A. Alvi, A. A. Al-Ghamdi, M. Husain, *Physica B* **2017**, *521*, 312–316.
- [19] J. Kennedy, F. Fang, J. Futter, J. Leveneuer, P. P. Murmu, G. N. Panin, T. W. Kang, E. Manikandan, *Diamond Relat. Mater.* **2017**, *71*, 79–84.
- [20] A. S. Elahi, M. Ghoranneviss, *Res. Phys.* **2017**, *7*, 1006–1009.
- [21] P. G. Freire, R. H. O. Montes, F. C. Romeiro, S. C. S. Lemos, R. C. Lima, E. M. Richter, R. A. A. Munoz, *Sens. Actuator B* **2016**, *223*, 557–565.
- [22] G. Fan, F. Li, D. G. Evans, X. Duan, *Chem. Soc. Rev.* **2014**, *43*, 7040–7066.
- [23] H. Chen, L. Hu, M. Chen, Y. Yan, L. Wu, *Adv. Funct. Mater.* **2014**, *24*, 934–942.
- [24] Z. Li, M. Shao, Q. Yang, Y. Tang, M. Wei, D. G. Evans, X. Duan, *Nano Energy* **2017**, *37*, 98–107.
- [25] M. Zhao, Q. Zhang, J. Huang, J. Nie, F. Wei, *Carbon* **2010**, *48*, 3260–3270.
- [26] M. Marco, R. Menzel, S. M. Bawaked, M. Mokhtar, A. Y. Obaid, S. N. Basahel, M. S. P. Shaffer, *Carbon* **2017**, *123*, 616–627.
- [27] W. Li, B. Gong, P. Wu, S. Yang, Q. Yang, Z. Dang, N. Zhu, *Appl. Clay Sci.* **2017**, *135*, 95–106.
- [28] S. Zhang, Y. Zhang, W. Jiang, X. Liu, S. Xu, R. Huo, F. Zhang, J. Hu, *Carbon* **2016**, *107*, 162–170.
- [29] L. Zhang, R. Chen, K. N. Hui, K. S. Hui, H. Lee, *Chem. Eng. J.* **2017**, *325*, 554–563.
- [30] H. Wang, X. Xiang, F. Li, *AIChE J.* **2010**, *56*, 768–778.
- [31] M. Lan, G. Fan, W. Sun, F. Li, *Appl. Surf. Sci.* **2013**, *282*, 937–946.
- [32] O. Saber, H. Tagaya, *Mater. Chem. Phys.* **2008**, *108*, 449–455.
- [33] H. P. Klug, L. E. Alexander, *X-ray Diffraction Procedures for Polycrystalline and Amorphous Materials*, Wiley, New York, **1954**.
- [34] C. Tang, Y. Tian, S. Hsu, *Materials* **2015**, *8*, 4895–4911.
- [35] G. Prabhavathi, M. Arjun, R. Yamuna, *J. Chem. Sci.* **2017**, *129*, 699–706.
- [36] C. He, C. Feng, J. Lin, E. Liu, C. Shi, J. Li, N. Zhao, *Acta Metall. Sin. (Engl. Lett.)* **2016**, *29*, 188–198.
- [37] O. Saber, *Polym. Bull.* **2012**, *68*, 209–222.
- [38] Y. Chen, Z. H. Huang, F. Yue Mand Kang, *Nanoscale* **2014**, *6*, 978–985.
- [39] J. Xu, S. Gai, F. He, N. Niu, P. Gao, Y. Chen, P. Yang, *Dalton Trans.* **2014**, *43*, 11667–11675.
- [40] G. Pyrgiotakis, W. M. Sigmund in *Nanostructured Materials and Nanotechnology II*, (Eds.: S. Mathur, M. Singh), John Wiley and Sons, Inc., New Jersey, **2009**, pp. 197.
- [41] F. Inoue, R. A. Ando, P. Corio, *J. Raman Spectrosc.* **2011**, *42*, 1379–1383.
- [42] M. Cargnello, M. Grzelczak, B. Rodríguez-González, Z. Syrgiannis, K. Bakhmutsky, V. L. Parola, L. M. Liz-Marzán, R. J. Gorte, M. Prato, P. Fornasiero, *J. Am. Chem. Soc.* **2012**, *134*, 11760–11766.
- [43] R. Nie, J. Shi, W. Du, W. Ning, Z. Hou, F. Xiao, *J. Mater. Chem. A* **2013**, *1*, 9037–9045.
- [44] J. Y. Gong, S. H. Yu, H. S. Qian, L. B. Luo, T. W. Li, *J. Phys. Chem. C* **2007**, *111*, 2490–2496.

Received: August 15, 2018